

Dynamic experimental study on single and double beam-column joints in steel traditional-style buildings

Jiayang Xue¹, Liangjie Qi^{*1,2}, Kun Yang¹ and Zhanjing Wu¹

¹Department of Civil Engineering, Xi'an University of Architecture and Technology, Xi'an 710055, China

²Department of Civil and Environmental Engineering, Virginia Tech, Blacksburg, 24060, USA

(Received March 4, 2017, Revised May 16, 2017, Accepted May 18, 2017)

Abstract. In order to study the failure mode and seismic behavior of the interior-joint in steel traditional-style buildings, a single beam-column joint and a double beam-column joint were produced according to the relevant building criterion of ancient architectural buildings and the engineering instances, and the dynamic horizontal loading test was conducted by controlling the displacement of the column top and the peak acceleration of the actuator. The failure process of the specimens was observed, the bearing capacity, ductility, energy dissipation capacity, strength and stiffness degradation of the specimens were analyzed by the load-displacement hysteresis curve and backbone curve. The results show that the beam end plastic hinge area deformed obviously during the loading process, and tearing fracture of the base metal at top and bottom flange of beam occurred. The hysteresis curves of the specimens are both spindle-shaped and plump. The ultimate loads of the single beam-column joint and double beam-column joint are 48.65 kN and 70.60 kN respectively, and the equivalent viscous damping coefficients are more than 0.2 when destroyed, which shows the two specimens have great energy dissipation capacity. In addition, the stiffness, bearing capacity and energy dissipation capacity of the double beam-column joint are significantly better than that of the single beam-column joint. The ductility coefficients of the single beam-column joint and double beam-column joint are 1.81 and 1.92, respectively. The cracks grow fast when subjected to dynamic loading, and the strength and stiffness degradation is also degenerated quickly.

Keywords: traditional-style buildings; dynamic test; double beam-column joints; peak acceleration; tearing fracture

1. Introduction

Ancient architectures are beautifully shaped with high cultural, historical and artistic value. Ancient building is simply constructed of wood or mainly by the wood loading structure using a variety of metal connectors or mortise-tenon means to connect and fix (Yang *et al.* 2000, Yao *et al.* 2006, Piazza *et al.* 2008, Yu *et al.* 2008). Because this kind of building is composed of natural material, it is restricted to the material itself. With the time changes, the destruction of such buildings is becoming increasingly serious, intact ones remain indeed scarce. Also, wood is more vulnerable to fire, and difficult to meet the larger, more complex space needs (Xue and Qi 2016). In order to inherit and promote the traditional culture, traditional-style buildings utilizing modern materials and construction technology comes into being and their appearances are consistent with ancient buildings. Due to light weight and high bearing capacity of steel material, it thus has been widely used in traditional-style buildings (Xue *et al.* 2016, Xue *et al.* 2016, Xue *et al.* 2016).

In ancient buildings, joints are divided into two groups, one is called single beam-column joint, and the other is double beam-column joint (Guo 1998). Fig. 1 shows the

instances of these two categories. To meet the modeling requirement, the column is erected as a circular cross section and the box section is used in the beam construction. The double beam-column joint is utilized in some landmark buildings, such as Chinatown in North America, Gyongbokkung in Korea, Danfeng Gate in China and so on.

The beam-column joint which transfers the shear force and bending moment is the main component of steel moment frame. The seismic behavior of steel structural box beam-circular column joint was studied using experimental and numerical investigation by many researchers. Tsai *et al.* (Tsai *et al.* 1995) assessed ten beam-to-wide-flange-column moment-connection specimens using bolted-web-welded-flange (BWFF), the ultimate beam-flange flexural strength accurately predicts the ultimate moment capacities of the BWFF connections. Lee *et al.* (2005) presented test results on eight reduced beam section (RBS) steel moment connections. Test results from this study showed that panel zones could easily develop a plastic rotation of 0.01 rad without causing distress to the beam flange groove welds. Leon *et al.* (1998) analyzed numerous unexpected fractures of welded steel moment-resisting frame connections in the Northridge Earthquake, then conducted cyclic experiment of bare steel full-scale specimens and the connections failed either brittlely at the welded interface of the bottom girder flange and the column flange, or with a low cycle fatigue failure emanating from the root of the bottom girder flange access hole. A series of six full-scale

*Corresponding author, Ph.D. Candidate
E-mail: qiliangjie@gmail.com



Fig. 1 The joints of ancient architecture

cruciform H-shaped beam to square tube column joint with cast steel stiffener specimens by Han *et al.* (2016). The results demonstrate that the joints with cast steel stiffeners have excellent moment capacity, deformation performance, and energy dissipation coefficients. A simple method was proposed to enhance the ductility of beam-to-column connections by Chen *et al.* (1996). The paper showed the ultimate strengths of the newly designed connections are almost unaltered by experimental study under cyclic load, whereas the stiffness is decreased only slightly. The fracture proneness of connections due to welding sensitivity and stress concentration from abrupt geometry alternation can be minimized and the energy dissipation capacity can be improved. Nakashima *et al.* (1998) described the results of cyclic loading tests applied to 14 full-scale beam-column subassemblages. Japanese practice for design and fabrication of beam-to-column connections was summarized, and efforts to improve connection performance in light of the damage to beam-to-column connections observed after the 1995 Kobe Earthquake were discussed. Shanmugam and Ting (1995) conducted experimental investigations to study the ultimate load behavior of I-beam to box-column connections stiffened externally. Results showed clearly that these connections satisfy the basic criteria: sufficient strength, sufficient rotation capacity, and adequate stiffness for a moment connection.

Components of steel traditional-style building use rigid connection method interacting with each other, while the

ancient wood building components are connected by mortise and tenon, which can be seen as semi-rigid connection (Tankut *et al.* 2003, Akcay *et al.* 2005, Erdil *et al.* 2005, Feio *et al.* 2014). When subjected to the strong earthquake, the rigid joints tend to be destroyed brittly due to cracking of weld joints. The traditional style building, constructed according to the relevant construction rules of the ancient architecture, has many special components and shape requirements compared with the modern frame structure, and its seismic performance is different from the conventional structure significantly (D'Ayala and Benzoni 2012). At the same time, because of the use of modern building materials and construction process, the seismic performance of traditional-style buildings is obviously different from the ancient buildings. As an important part of structural force transmission, beam-column joints should be focused on experimental and theoretical research. However, the research on traditional style architecture is rather few at present (Li 2014, Zhang 2015, Xie *et al.* 2016, Xue *et al.* 2016) and the theory system needs to be improved. What's more, the existing studies are all about static test study, which the human intervention is fairly strong and cannot reflect to the dynamic response of the structures when subjected to actual earthquake wave.

In order to provide theoretical guidance for the application of steel traditional-style buildings, one single beam-column joint and one double beam-column joint are fabricated according to the principle of "strong column and weak beam", so as to compare the seismic performance of two different types of joints in traditional-style architecture subjected to earthquake. In addition, the dynamic loading procedure is utilized to load the specimens. The damage mode and seismic performance of the joint are compared and analyzed, which could provide a reference for the theoretical research and engineering design of the steel traditional-style building.

2. Experiment program

2.1 Test specimen

Two specimens were fabricated based on the engineering instance of a traditional-style building, and the size changed according to the relevant regulations of Building Standards of Song Dynasty (Liang and Wilma 1984). The specimen was made as 1/2.6 models, in which single beam-column joint numbered SBJ-1 and the double beam-column was DBJ-1. The steel used in this test was Q235B and all beam-column connections were welded, the fillet weld was used when connecting thin plates and penetration groove welding method for thick plates. The E43 welding electrodes were adopted according to the Steel Structure Design Codes (GB 50017-2003).

Since the test is a destructive test and the specimens are designed according to "strong column and weak beam" principle, the wall thickness of square steel column and round steel pipe is much larger than that of box-section beam. The basic parameters of the specimen are shown in Table 1. The following steps are followed during the production procedure of the test pieces: Welding the box

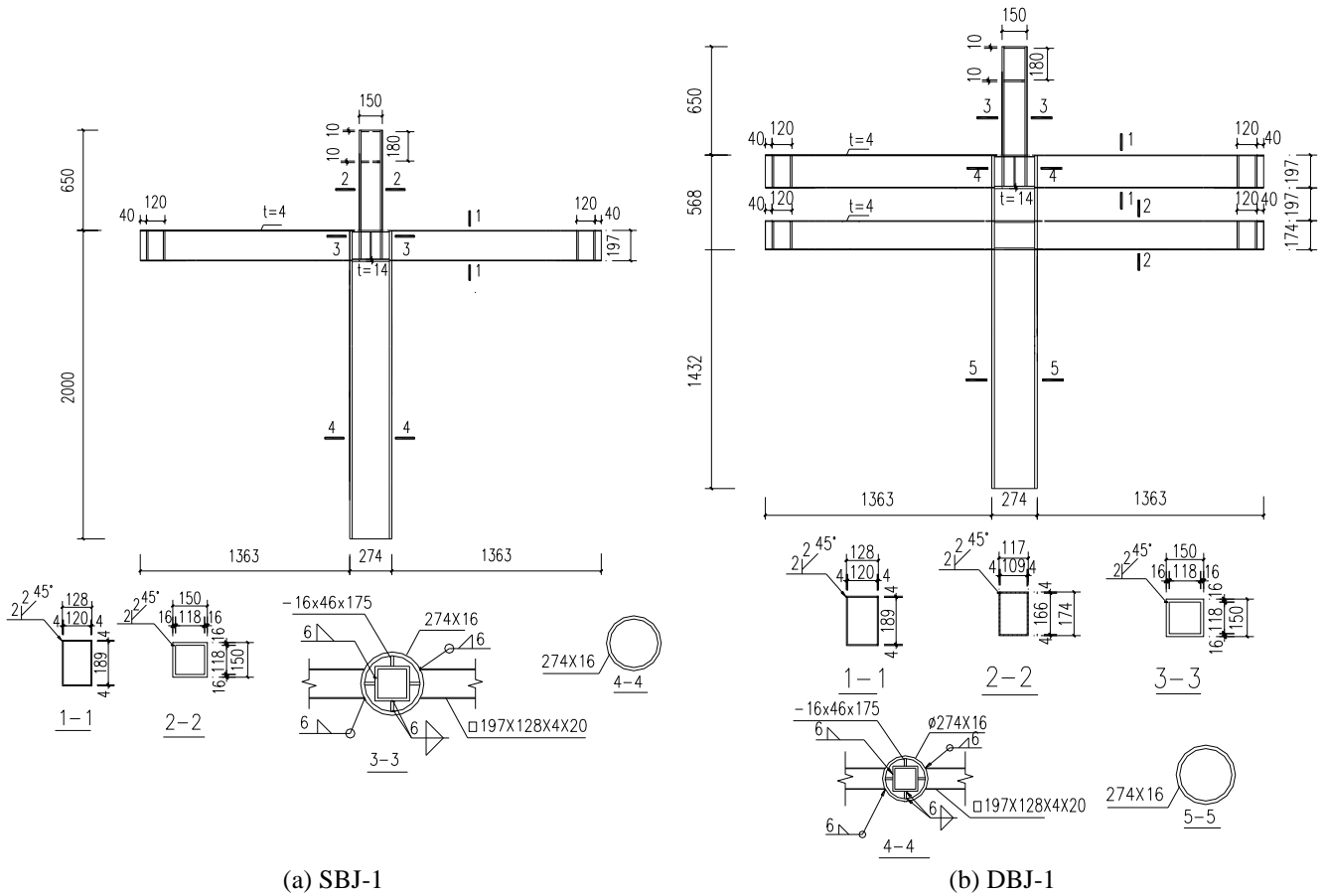


Fig. 2 Dimensions and details of specimens

Table 1 Design parameters of specimens

Specimen	Axial compression ratio	Top beam		Bottom beam		Circular steel pipe (mm)	Square steel tube (mm)
		Flange (mm)	Web (mm)	Flange (mm)	Web (mm)		
SBJ-1	0.3	128×4	197×4	—	—	274×16	150×16
DBJ-1	0.3	128×4	197×4	117×4	174×4	274×16	150×16

Table 2 Steel mechanical indexes

Category	Wall thickness t/mm	Yield strength f_y /MPa	Ultimate strength f_u /MPa	Elastic modulus $E_s/10^5$ MPa	Elongation δ /%	Yield strain $\epsilon/10^{-6}$
Tube	16	283.4	415.3	2.05	34.5	1383
Plate	16	277.2	412.6	2.01	37.2	1379
Plate	4	275.9	402.1	1.98	35.1	1393

beam→Welding the square steel column→Assembling and welding the square steel column and the circular steel column→Assembling and welding the beam and column.

The sample used in the circular steel pipe is the seamless steel pipe, at the same time, square steel column and the box beam are welded together by four steel plates. All of the members are welded and in strict accordance with the construction requirements and the welding process in “Steel Structure Design Code” (GB 50017-2003) and “Welding Specification of Steel” (GB50661-2011). The items in these specifications states that the rational groove shape and size should be based on different welding method. When the base metal thickness is less or equal to 6 mm, the fillet leg size should be no less than 3 mm. The top beam parallels the bottom beam with a distance of 197mm. The total height of the specimen is 2650 mm and the width is 3000 mm. The geometry and detailed construction of the specimen are shown in Fig. 2. The material mechanical characteristics are shown in Table 2. Table 3 shows the section capacities of the members.

2.2 Test setup

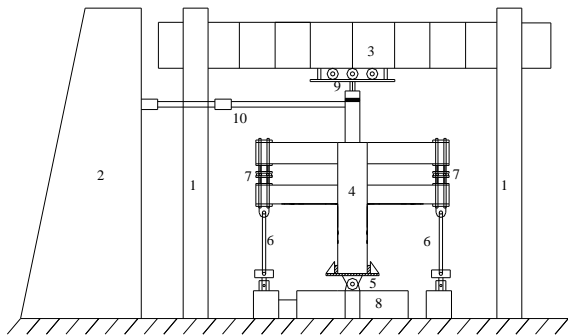
In the test, the vertical load was applied to the top of the column by the hydraulic jack, then keeping the designed value during the whole test. The horizontal dynamic load on the column end was controlled by 500 kN electro-hydraulic servo which was installed on the reaction wall. The horizontal actuator has a range of ±250 mm. The whole testing process was controlled by the MTS973 electro-hydraulic servo testing system.

Based on the constraints and force conditions of the actual structure, the loading restraint device of the test

Table 3 Section bearing capacities

Specimen	Members	A (mm ²)	I ($\times 10^7$ mm ⁴)	S ($\times 10^5$ mm ³)	Z ($\times 10^5$ mm ³)	M_n (kN·m)	M_a (kN·m)
SBJ-1	Single beam	2536	1.40	1.14	1.70	26.79	31.45
	Rectangular column	8576	2.60	2.89	4.33	67.92	80.11
	Top beam	2536	1.40	1.14	1.70	26.79	31.45
DBJ-1	Bottom beam	2264	0.98	0.90	1.35	21.15	24.83
	Rectangular column	8576	2.60	2.89	4.33	67.92	80.11

Note: A , I , S , Z and M are the area, moment of inertia, elastic section modulus, plastic section modulus and bending moment of the cross-section, respectively. Subscripts n and a represent capacities using nominal and actual material properties, respectively.



(a) Sketch



(b) On-site picture

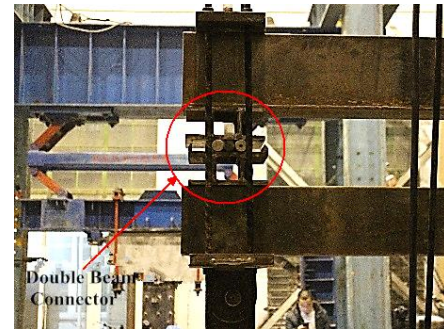
1. Reaction frame 2. Reaction wall 3. Reaction beam
4. Specimen 5. Hinge support 6. Vertical tension rod 7.
Connector of double beams 8. Ground beam 9. Vertical
jack 10. Horizontal actuator

Fig. 3 Test setup

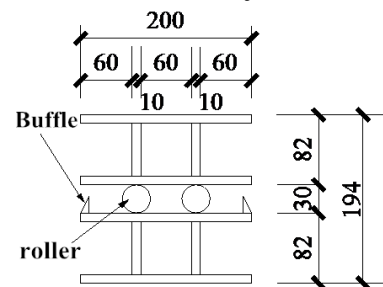
specimen was designed. The beam end was connected to the ground beam using a tie rod, and the column bottom was restrained by a fixed hinge support. The axial load was applied in the vertical direction at the column top end, and the cyclic load was applied horizontally. The loading devices of the two specimens were basically the same, except the double-beam connector was installed to ensure the bare horizontal displacement of the beam flange in the double-beam column loading test. Fig. 3 shows the schematic diagram and on-site of the loading device of the specimen. The double beam connector is exhibited in Fig. 4.

2.3 Loading system

In order to better simulate the earthquake effect, the dynamic loading mode was selected during the experiment



(a) Real object



(b) Detailed size

Fig. 4 Connector of double beam

(Niwa *et al.* 2000). Given that the seismic wave can be seen as a collection of sine waves of different frequencies, so the sine acceleration waveform was adopted. The layer displacement angle of the steel structure in Seismic Design Code is also provided: elastic interstory drift angle limit is 1/250 and elastic-plastic interlayer displacement angle limit is 1/50, respectively. Then the interlayer displacement angle corresponding to different seismic intensity was determined based on this specification, and the top control displacement corresponding to each loading condition was obtained by conversion. At the same time, considering the influence of loading acceleration on the stress of the specimen, the peak acceleration corresponding to each earthquake intensity was acquired according to Chinese Seismic Intensity Scale (GB/T 17742-2008), which showed the peak acceleration corresponding to various seismic intensity, as shown in Table 4. Finally, the loading frequency of each sine wave was obtained by the peak acceleration and the control displacement. Then the loading system of this experiment was completed. The dynamic loading procedure is shown in Table 5, and each loading mode is cycled five times. The specific loading scheme is illustrated in Fig. 5.

Table 4 seismic intensity scale of China

Seismic intensity	VI	VII	VIII	IX
Horizontal peak acceleration (m/s^2)	0.45~0.89	0.90~1.77	1.78~3.53	3.54~7.07

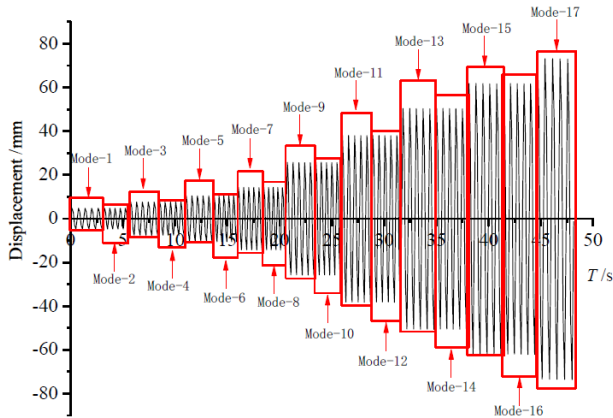


Fig. 5 Loading scheme

The dynamic data of the strain gauges were collected from 8-channel dynamic strain data acquisition instrument. All the eight strain gauges were arranged at the plastic hinge region and the core region of the joint because the deformation of the specimen is mainly concentrated on the plastic hinge region. Fig. 6 illustrates the layout of the tested points of SBJ-1 and DBJ-1. The displacement and load at the top of specimens are automatically collected by the MTS973 loading system.

3. Damage evolution and failure modes

3.1 Loading process

Before the test, the axial load of 600 kN (axial compression ratio of 0.3) was applied to the column end, and then the rods on both ends of the specimen were installed. Finally, a horizontal dynamic load was applied to the column end.

The test specimen is designed based on the principle of “strong column and weak beam”. Therefore, the damage phenomena of the plastic hinge zone at the beam end are

obvious during the test. There is no obvious change in the core area of the joint. The destruction process of each specimen is described below.

3.1.1 SBJ-1

The bearing load was from -22.26 kN to 20.18 kN and the maximum displacement of column end was 14.33 mm in the loading stage from Loading Mode 1 to Loading Mode 8. The strain values were all lower than the yield strain of the steel. In the meantime, the load-displacement curve of the column end changed linearly, and the joint was still in the elastic working stage. Then the specimen yielded at Mode 9, the maximum load of two loading direction was 37.48 kN and -31.52 kN, respectively, and the corresponding displacement was 26.58 mm and -23.22 mm, respectively.

The specimen moved cyclically during the dynamic loading stage. When the column ends reached the maximum displacement during each cycle, the column tilted and the center of each beam buckled, while two beams curved in the opposite direction. With the increase of the external loading, the buckling deformation of the plastic hinges area became more significant, and the top flange and the webs of the beams were concave and convex successively. When loaded to Mode 13, the weld at the beam-to-column connection cracked. Then at Mode 14, the base metal at the webs of east beam and southern web of the west beam torn, at the same time, the weld at the connection of west beam and column cracked completely. Test ended after SBJ-1 specimen loaded into Loading Mode 17, crack penetration at the top flange of both beams showed up and the base metal of the webs cracked along the oblique 45 degree. The ultimate failure mode of the SBJ-1 specimen is shown in Fig. 7.

3.1.2 DBJ-1

The DBJ-1 specimen also yielded at the Mode 9. Compared with SBJ-1, the absolute load value of column end was a little higher than SBJ-1 and the maximum absolute displacement was 14.41 mm during Loading Mode 1 to Mode 8. At Loading Mode 9, the maximum load at each direction is 51.39 kN and -52.17 kN, respectively, which is higher than that of SBJ-1.

With the increase of the load, concave and convex deformation showed up at the top flange of the upper and

Table 5 Loading mode

Mode	Intensity	Peak acceleration (m/s^2)	Displacement (mm)	Mode	Intensity	Peak acceleration (m/s^2)	Displacement (mm)
1	VII	0.50	5	10	IX1	4.25	27
2	VI2	0.80	5	11	IX2	4.60	40
3	VIII1	1.00	8	12	IX3	4.80	40
4	VII2	1.25	8	13	IX4	5.00	53
5	VII 3	1.50	11	14	IX5	5.50	53
6	VIII1	2.00	11	15	IX6	5.70	65
7	VIII2	2.50	15	16	IX7	5.78	65
8	VII3	3.00	15	17	IX8	5.85	77
9	VIII4	3.50	27	18	IX9	5.93	77

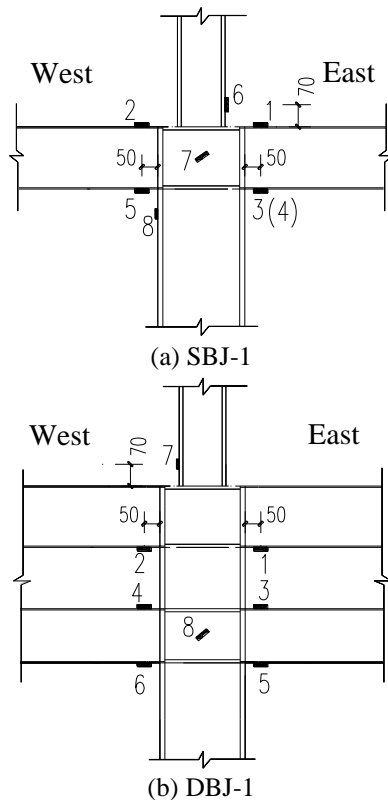


Fig. 6 Measurement points layout

lower beam. When loaded to the Mode 14, the base material of the top flange of the west upper beam first torn and then extended to the web. In the subsequent loading process, other cracking phenomenon occurred at other members. At the same time, the base material crack length and width also continued to grow until base metal of the beam flange completely torn, then the loading stopped. The DBJ-1 specimen was loaded until the Loading Mode 17, and its ultimate failure mode was the severe buckling at the plastic hinge region of the beam-column connection. What's more, the base metal of the upper flange was almost broken completely. The ultimate failure mode of DBJ-1 specimen is shown in Fig. 8.

3.2 Failure modes

(1) The failure was mainly occurred at the plastic hinge

area of connections. During the whole loading process, the deformation concentrated on the beam hinge region, which was about 5-10 cm from the column surface. The deformation of the plastic hinge zone was rather small before yielding, but the deformation aggravated significantly during the later loading process. The buckling deformation was observed on the both flanges and the webs. With the increase of dynamic load and the displacement, the base metal at plastic hinge region torn apart and extended to webs, however, no obvious deformation of the column and the core area showed up during the whole loading process.

(2) After plastic deformation appeared in the plastic hinge area, the failure of the SBJ-1 specimen was due to the failure of the weld which was at the top flange of upper beams, and then crack occurred about oblique 45 degree on both sides of the web. However, as for DBJ-1 specimen, the base metal which was 5-10 cm from the joint sides first torn, then some crack occurred at the top flange and webs. In the following push-pull reciprocating dynamic load, the crack of base metal opened and closed constantly, which led to some damage of vertical weld. At the same time, the crack at the flange edge extended to the middle part of the flange. At the end of the experiment, the beam flange base metal cracked thoroughly.

(3) The above phenomenon belongs to the scope of ductile failure, the ductile fracture process contains those stages of micro void nucleation, growth and coalescence. Voids nucleate as a result of debonding of secondary particles or inclusions from the steel matrix when sufficient stresses are applied (Wang *et al.* 2011). And it is in close relationship with strain rate effect and loading rate effect.

4. Results and discussion

4.1 Strain analysis

4.1.1 SBJ-1

The strain gauges of 1, 2, 3, 5 (plastic hinge at the beam end), 7 (core area of joint) and 8 (circular steel tube) are selected to analyze the strain development from Loading Mode 1 to Mode 10. The load-strain curves between Mode 1 to 10 are shown in Fig. 9.

The following can be seen from Fig. 9.

(1) The strain value of the plastic hinge region at the beam end increases rapidly with the increase of the loading.



(a) West beam



(b) East beam



(c) Top flange



(d) Plastic hinge region

Fig. 7 Failure pattern of SBJ-1

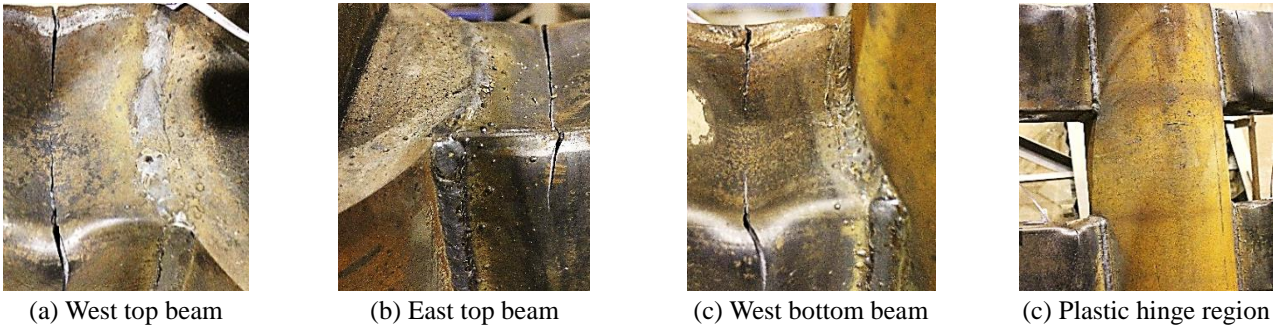


Fig. 8 Failure pattern of DBJ-1

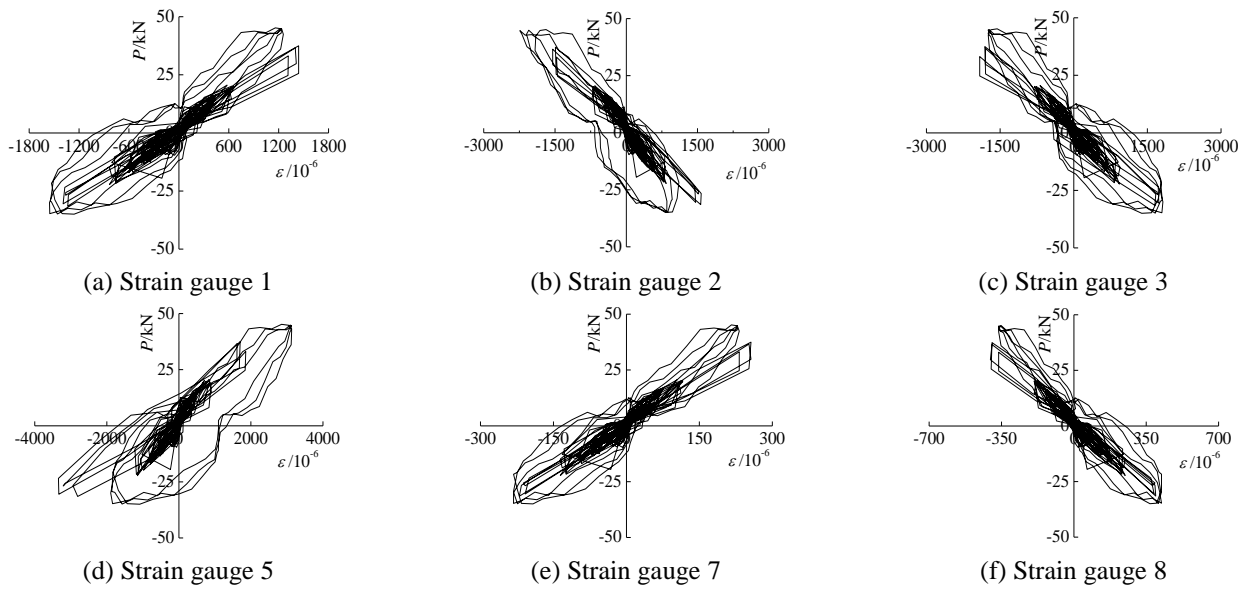


Fig. 9 Load-strain curves of SBJ-1

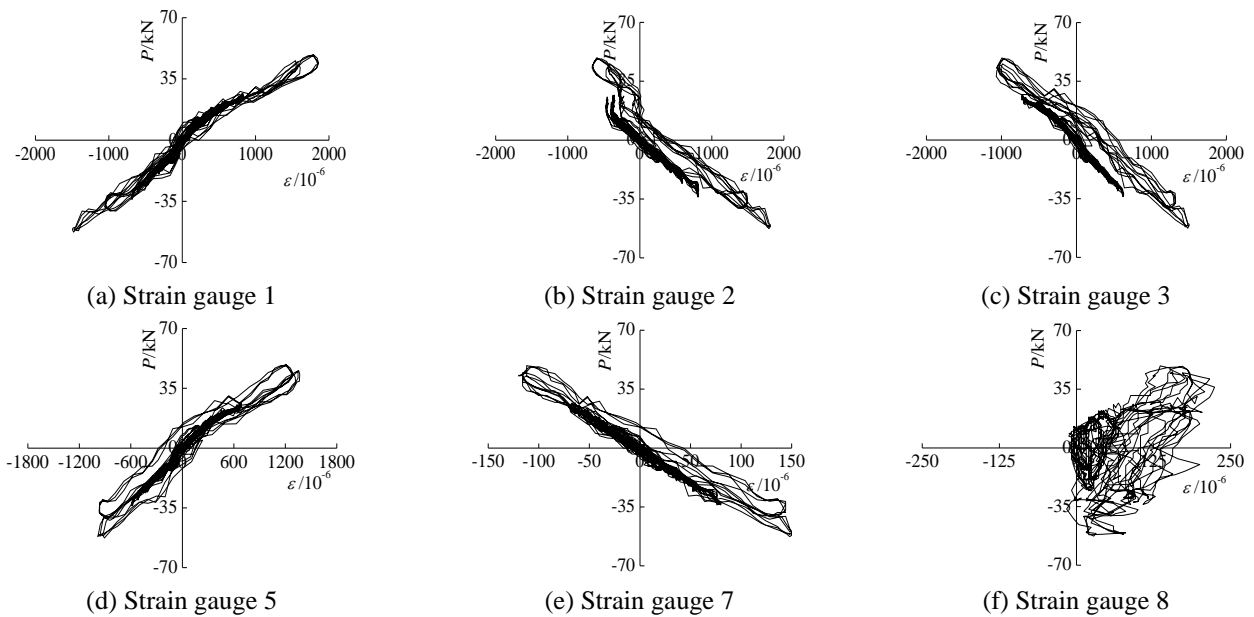


Fig. 10 Load-strain curves of DBJ-1

At Loading Mode 8, The maximum strain values of strain gauges 1, 2, 3, 5 are $836 \mu\epsilon$, $828 \mu\epsilon$, $944 \mu\epsilon$ and $1068 \mu\epsilon$, respectively, and the plastic hinge area at the beam end has

not yielded. At Loading Mode 9, the maximum strain values of strain gauges 1, 2, 3 and 5 are $1440 \mu\epsilon$, $1576 \mu\epsilon$, $1916 \mu\epsilon$ and $3344 \mu\epsilon$, respectively, surpassing the yield strain value,

the specimen enters the elastoplastic working stage. The buckling deformation of the plastic hinge region at the beam end is obvious and the rapid development can be observed.

(2) The strain gauge 7 (core area of the joint) and the strain gauge 8 (circular steel tube) were below $500 \mu\epsilon$ before Loading Mode 10, and they did not yield in the whole loading process. From the experimental phenomena, no visible deformation of the circular tube, square steel column and the core area appeared. All of these indicate that the columns and the core area are always in the elastic working phase during the loading process.

4.1.2 DBJ-1

The load-strain curves of DBJ-1 between Mode 1 to 10 are exhibited in Fig. 10.

From the figures, it can be seen as follows.

(1) At Loading Mode 8, the maximum strain of strain gages 1, 2, 3 and 5 is $812 \mu\epsilon$, $824 \mu\epsilon$, $564 \mu\epsilon$, $672 \mu\epsilon$, respectively, which means the strain-load curves show a linear increase in the early stage of loading. When loaded to Mode 9, the maximum strain is $1608 \mu\epsilon$, $1848 \mu\epsilon$, $1564 \mu\epsilon$ and $1428 \mu\epsilon$, respectively, which demonstrate the plastic hinge area of the beam end yield and the specimen enters the elastic-plastic working stage. In the mean time, the plastic hinge zone strain of top beam is larger than that of the bottom beam. When compared with these two specimens, the strain value of the plastic hinge region is not much different. However, the bearing capacity of DBJ-1 is higher than that of SBJ-1 under the same mode.

(2) The strain values of the square column and the core area of the specimen are less than $250 \mu\epsilon$ subjected to the Mode 9, and the yield phenomenon is not observed in the whole loading process, which indicates that the column and the core joint is in the elastic stress stage, and it meets seismic design requirements of "strong column-weak beam".

4.2 Hysteretic loops

The load-displacement hysteresis curves are shown in Fig. 11, where P is the horizontal load at the column end and Δ is the corresponding horizontal displacement. They have the following characteristics:

(1) Before the plastic hinge area yielded, the load-displacement curves cycled along a straight line basically and the specimen was in elastic stage. The hysteresis loop area is relatively small, and no stiffness degradation and residual deformation are observed.

(2) With the increasing of load, buckling phenomenon emerged at the plastic hinge area. Correspondingly, the hysteresis curves were roughly spindle-shaped and gradually became plump, showing remarkable energy-consuming characteristics. In addition, a larger residual deformation began to appear. The initial slope decreased gradually, which indicates that the stiffness of the specimen is deteriorating with the plastic deformation aggravating of the plastic hinge region and the continuous development of cracks.

(3) By comparing the hysteresis curves of the two

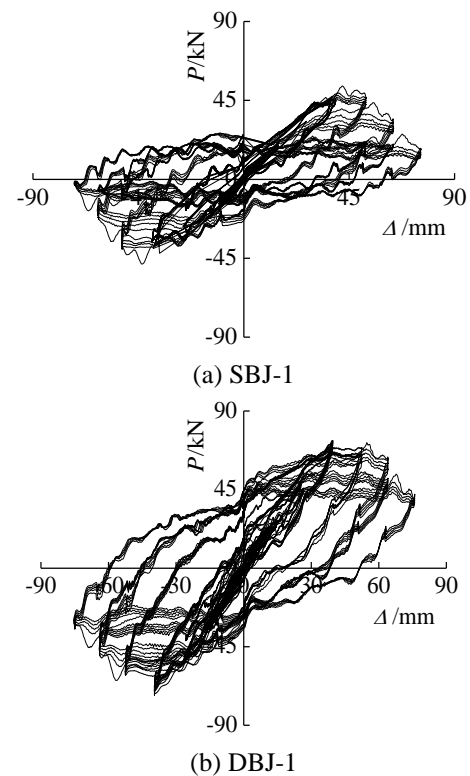


Fig. 11 Hysteretic loops of specimens

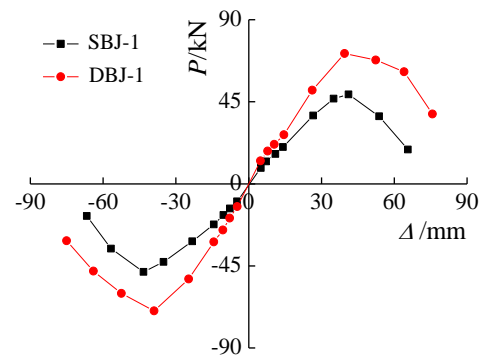


Fig. 12 Backbone curves

specimens, it can be found that the hysteresis loop area and ultimate load of the DBJ-1 are significantly higher than those of the SBJ-1.

(4) Under the dynamic load effect, the hysteresis curve of the specimen fluctuated up and down. That was because pump and valve capacity couldn't match the loading acceleration requirement, and the output signal was not consistent with the input command very well. The load decreases rapidly after the specimen reaches the ultimate bearing capacity, and the strength decay and the stiffness degradation are remarkable.

(5) Each load was carried out cyclically for five consecutive times under the same loading mode, it can be seen that the hysteresis curves of five cycles do not coincide with each other in the same loading condition. The load is significantly reduced when keeping the loading displacement the same. This is because the specimen enters into the plastic deformation stage, the residual deformation

and cumulative damage are produced under each loading cycle, then the bearing capacity and energy dissipation capacity of the specimen are reduced.

4.3 Backbone curves

The backbone curve is an important indicator of the seismic performance of structures. Based on the hysteresis curves of the test specimen, the backbone curves of SBJ-1 and DBJ-1 are obtained, as shown in Fig. 12.

Some load-displacement features could be acquired by the backbone curves.

(1) Before the yielding mode, there was a linear relationship between load and displacement, the specimen is still in the elastic stage. When the specimen starts to yield, the slope of the skeleton curve decreases, the deformation develops faster than the load growth, and the stiffness decreases rapidly. After the ultimate load-carrying capacity of the specimen, the bearing capacity decreases with the increase of the displacement. The descending section of the skeleton curve appears due to the appearance of the base material tearing and the weld cracking.

(2) Compared with SBJ-1, DBJ-1 has greater lateral stiffness and stronger load-bearing capacity. The ultimate load of the DBJ-1 is much larger than that of the SBJ-1, however, the ultimate displacements of the two specimens keep the same value.

(3) After the ultimate load-carrying capacity, the fracture of the base metal is commonly observed in the plastic hinge area of beam ends. Owing to the rapid velocity of dynamic loads, the cracks develops extremely fast, but that of DBJ-1 is slower than SBJ-1.

4.4 Characteristic values

The yield point and the corresponding displacement can be determined by using the General Yielding Bending Moment Method (Liu *et al.* 2014). According to China's Industry Standard "Building Seismic Test Method" (JGJ101-96), the ultimate point should take the point on backbone curve when the load drops to 85% of the maximum load.

The experimental values of the characteristic points are shown in Table 6, where P_y , P_m and P_u stand for the yield load, maximum load and ultimate load, respectively, Δ_y , Δ_m and Δ_u are the displacements corresponding to the load P_y , P_m and P_u . The ductility coefficient μ is defined as $\mu = \Delta_u / \Delta_y$.

From the above table, the following can be drawn.

(1) The yield load, maximum load and ultimate load of

DBJ-1 are 49.5%, 45.1% and 44.6% higher than SBJ-1, respectively. The yield displacement and maximum displacement of SBJ-1 and DBJ-1 are almost the same, but the ultimate displacement of DBJ-1 is larger than that of SBJ-1. This is because the crack failure of SBJ-1 appeared after it reached the maximum load-carrying capacity.

(2) The average values of ductility coefficients of DBJ-1 and SBJ-1 are 1.81 and 1.92, respectively. The ductility coefficients of the two specimens are relatively low and the difference is not significant. Due to the fast loading of test, the plastic deformation and fracture of the specimen developed rapidly under the action of dynamic load, which greatly reduced the ductility of the specimen.

(3) The interlayer yield displacement angles of SBJ-1 and DBJ-1 are 1/96 and 1/94, respectively. The ultimate displacement angles of DBJ-1 and DBJ-1 are 1/53 and 1/49, the deformability of DBJ-1 is slightly better than SBJ-1. According to "Seismic Design Code of Buildings" (GB50011-2010), the limit value of elastic displacement angle $[\theta_e]$ equals 1/250, and the elastoplastic limit value $[\theta_p]$ equals 1/50. It can be seen that the yield displacement angle of the test specimen, on the one hand, is much higher than the requirement, and the ultimate drift ratio is close to the limit value, which means that this kind of joints owns great deformability. On the other hand, the deformation of the specimen subjected to the dynamic load develops faster than that of static load.

4.5 Energy dissipation capacity

The energy dissipation capacity is an important index to evaluate the seismic performance of structural systems and is a direct representation of the energy absorption and dissipation (Ma *et al.* 2015). The energy dissipated by a structure or member in a loading cycle is equal to the area enclosed by a hysteresis loop.

The hysteretic energy (hysteresis loop area) of the SBJ-1 and the DBJ-1 under the odd-numbered loading mode is shown in Fig. 13.

In this paper, the equivalent viscous damping coefficient h_e is used to evaluate the energy dissipation capacity of the steel traditional-style joints. It is calculated using Equation (1) to evaluate the accurate energy dissipation ability of the specimens. $S_{(ABC+CDA)}$ is the area of the shadow and $S_{(OBE+ODF)}$ is represented by the sum of the area of the

Table 6 Characteristic values and ductility coefficients

Specimen	Yield point		Maximum point		Ultimate point		μ
	P_y /kN	Δ_y /mm	P_m /kN	Δ_m /mm	P_u /kN	Δ_u /mm	
SBJ-1	38.6	27.6	49.0	38.8	41.8	48.9	1.77
	-35.7	-27.6	-48.3	-39.3	-41.1	-50.9	1.84
DBJ-1	55.4	28.8	71.5	39.5	60.7	54.5	1.89
	-55.5	-27.4	-69.7	-39.0	-59.2	-53.2	1.94

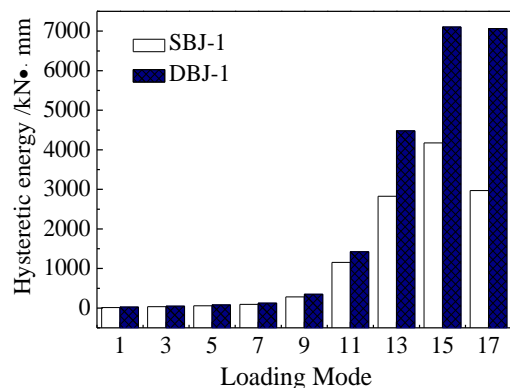


Fig. 13 Hysteretic energy

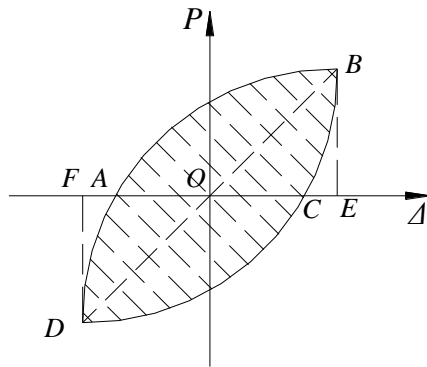


Fig. 14 Calculation of energy dissipation capacity

Table 7 Equivalent viscous damping coefficients

Specimen	h_9	h_{11}	h_{13}	h_{15}
SBJ-1	0.051	0.119	0.231	0.378
DBJ-1	0.045	0.080	0.213	0.427

triangle OBE and triangle ODF as shown in Fig. 14.

$$h_e = S_{(ABC+CDA)} / (2\pi \cdot S_{(OBE+ODF)}) \quad (1)$$

The equivalent viscous damping coefficients h_9 , h_{11} , h_{13} and h_{15} were calculated respectively corresponding to the Load Mode 9, 11, 13 and 15. The results are shown in Table 7.

The following can be found from the data in Table 6.

(1) The hysteretic energy dissipation and the equivalent viscous damping coefficient increase with the loading condition. The damping coefficients are above 0.2 under Loading Mode 13, which shows a good energy dissipation ability.

(2) The equivalent viscous damping coefficient of DBJ-1 is smaller than that of SBJ-1, because the plastic development of SBJ-1 is more remarkable under the same loading mode.

(3) It can be seen from the change tendency that there is no much difference between the hysteretic energy dissipation of two specimens before yielding (condition 9). After the yielding, the hysteretic energy dissipation of DBJ-1 is significantly larger than that of SBJ-1. And the hysteretic energy dissipation of SBJ-1 decreases obviously from the condition 15, while no such phenomenon is observed in DBJ-1.

4.6 Stiffness degradation and strength degeneration

After the structure enters the plastic state, the load capacity and the stiffness reduce with the increase of the repeated load under the condition that the displacement amplitude does not change (Xue *et al.* 2016). This characteristic is called strength degradation and stiffness degeneration.

In this paper, the strength degradation is expressed by the load-bearing capacity reduction coefficient λ_i , which is the ratio of the peak load of the last cycle to the peak load of the first cycle under the same loading mode. The stiffness degradation takes secant stiffness of the same mode to

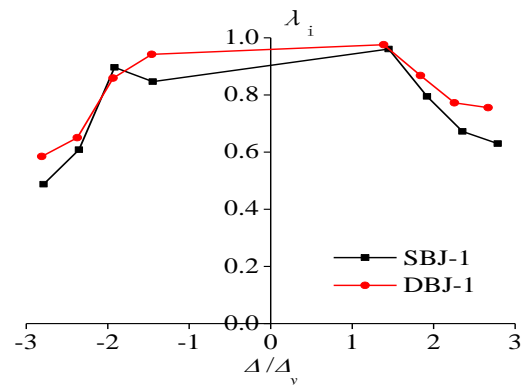


Fig. 15 Strength degeneration

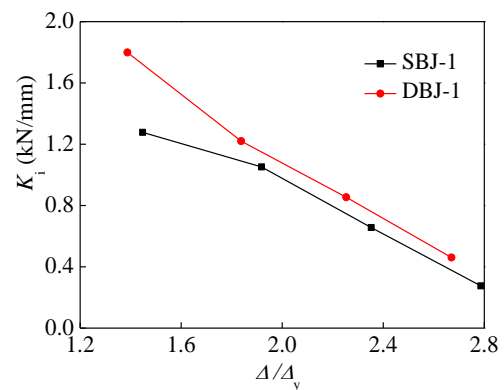


Fig. 16 Stiffness degradation

express. The secant stiffness is taken as the mean value of the five-cycle secant stiffness at the same loading mode.

The strength degradation coefficient and the secant stiffness versus the loading displacement level Δ/Δ_y are shown in Fig. 15 and Fig. 16, respectively.

From the above chart, the following can be seen.

(1) The strength and stiffness degenerate rapidly after yielding under the dynamic load condition.

(2) The reduction coefficient of the bearing capacity before reaching the maximum load is about 0.9, and the strength degradation is not obvious. After reaching the maximum load condition, the strength degradation is faster owing to the occurrence of crack of base metal and weld. In addition, the strength degradation speed of DBJ-1 is slower than that of SBJ-1.

(3) The stiffness after yielding shows a decline trend with the increase of displacement, and the primary cause of the stiffness degradation is the plastic deformation and cumulative damage of plastic hinge region, such as yielding of steel, plastic and the development of base metal and weld cracking. At the same loading mode, the secant stiffness of DBJ-1 is larger than that of SBJ-1, because the bearing capacity of DBJ-1 is significantly higher than that of SBJ-1 under the same loading displacement.

5. Conclusions

(1) The significant deformation and ultimate failure of the two specimens occurred in the plastic hinge region at

the beam end. At the last moment, the plastic hinge region at the beam end suffered serious buckling and tearing. During the whole loading process, the core area and columns were always in the elastic working stage and no obvious deformation appeared.

(2) The hysteresis curve of the specimen subjected to the dynamic load is wavy-shaped. However, the hysteresis curve of the DBJ-1 is plumper than that of the SBJ-1. The lateral stiffness and load-carrying capacity of DBJ-1 are significantly higher than those of SBJ-1.

(3) The strength decay and the stiffness degrade remarkably after the hysteresis curve of reaching the ultimate load-carrying capacity. The ductility coefficients of SBJ-1 and DBJ-1 are 1.81 and 1.92, respectively, and no significant difference is shown, which is mainly due to the faster speed of loading, the plastic deformation and the fracture of the base metal develops rapidly subjected to dynamic load, resulting in rapid decline in bearing capacity, and the deformation capacity is poor.

(4) Under the same working conditions, the hysteresis energy dissipation of SBJ-1 and DBJ-1 is similar and relatively small. After the yielding, the energy consumption of DBJ-1 is significantly higher than SBJ-1. The equivalent viscous damping coefficients of the two specimens are both above 0.2, so the energy dissipation capacity is great.

(5) Compared with single beam-column joints, double beam-column joints have the higher bearing capacity, more ductile damage phenomenon and slower strength degradation, which implies that double ones are more applicable in the high seismic intensity area.

Acknowledgements

The author would like to thank the support provided by the National Natural Science Foundation of China (Grant No. 51678478), National Science and Technology Support Program of the 12th Five-Year (Grant no. 2014BAL06B03), the Technology Research Task of China State Construction Engineering Corporation (Grant No. CSCEC-2012-Z-16) and Scientific Research Foundation of Outstanding Doctoral Dissertation of XAUAT (Grant no. 6040317006). Financial support from the China Scholarship Council for Liangjie Qi's work at Virginia Tech, as a visiting scholar, is highly appreciated.

Reference

- Akçay, H., Eckelman, C. and Haviarova, E. (2005), "Withdrawal, shear, and bending moment capacities of round mortise and tenon timber framing joints", *Forest Prod. J.*, **55**(6), 60-67.
- Chen, S.J., Yeh, C. and Chu, J. (1996), "Ductile steel beam-to-column connections for seismic resistance", *J. Struct. Eng.*, **122**(11), 1292-1299.
- D'Ayala, D. and Benzoni, G. (2012), "Historic and traditional structures during the 2010 Chile earthquake: observations, codes, and conservation strategies", *Earthq. Spectra*, **28**(S1), S425-S451.
- Erdil, Y., Kasal, A. and Eckelman, C. (2005), "Bending moment capacity of rectangular mortise and tenon furniture joints", *Forest Prod. J.*, **55**(12), 209-213.
- Feio, A.O., Lourenço, P.B. and Machado, J.S. (2014), "Testing and modeling of a traditional timber mortise and tenon joint", *Mater. Struct.*, **47**(1-2), 213-225.
- Guo, Q. (1998), "Yingzao Fashi: twelfth-century Chinese building manual", *Arch. History*, **41**, 1-13.
- Han, Q.H., Liu, M.J., Lu, Y. and Zhao, S.S. (2016), "Experimental and simulation study on seismic behavior of beam-column joints with cast steel stiffener", *J. Struct. Eng.*, **142**(7), 1-18.
- Lee, C.H., Jeon, S.W., Kim, J.H. and Uang, C.M. (2005), "Effects of panel zone strength and beam web connection method on seismic performance of reduced beam section steel moment connections", *J. Struct. Eng.*, **131**(12), 1854-1865.
- Leon, R.T., Hajjar, J.F. and Gustafson, M.A. (1998), "Seismic response of composite moment-resisting connections. I: Performance", *J. Struct. Eng.*, **124**(8), 868-876.
- Li, P. (2014), *Experimental Study on Seismic Behavior of RC Column-beam Joint Built in Traditional Style*, Xi'an University of Architecture and Technology, Xi'an.
- Liang, S. and Wilma, F. (1984), *A Pictorial History of Chinese Architecture*, MIT Press, Cambridge, Mass.
- Liu, Z.Q., Xue, J.Y., Zhao, H.T. and Gao, L. (2014), "Cyclic test for solid steel reinforced concrete frames with special-shaped columns", *Earthq. Struct.*, **7**(3), 317-331.
- Ma, H., Xue, J., Liu, Y. and Zhang, X. (2015), "Cyclic loading tests and shear strength of steel reinforced recycled concrete short columns", *Eng. Struct.*, **92**, 55-68.
- Nakashima, M., Suita, K., Morisako, K. and Maruoka, Y. (1998), "Tests of welded beam-column subassemblies. I: Global behavior", *J. Struct. Eng.*, **124**(11), 1236-1244.
- Niwa, N., Kobori, T., Takahashi, M., Midorikawa, H., Kurata, N. and Mizuno, T. (2000), "Dynamic loading test and simulation analysis of full-scale semi-active hydraulic damper for structural control", *Earthq. Eng. Struct. Dyn.*, **29**(6), 789-812.
- Piazza, M., Baldessari, C. and Tomasi, R. (2008), "The role of in-plane floor stiffness in the seismic behaviour of traditional buildings", *14th World Conference on Earthquake Engineering*, Beijing, China.
- Shanmugam, N. and Ting, L. (1995), "Welded interior box-column to I-beam connections", *J. Struct. Eng.*, **121**(5), 824-830.
- Tankut, A., Denizli-Tankut, N., Gibson, H. and Eckelman, C. (2003), "Design and testing of bookcase frames constructed with round mortise and tenon joints", *Forest Prod. J.*, **53**(7/8), 80-86.
- Tsai, K., Wu, S. and Popov, E.P. (1995), "Experimental performance of seismic steel beam-column moment joints", *J. Struct. Eng.*, **121**(6), 925-931.
- Wang, Y., Zhou, H., Shi, Y. and Xiong, J. (2011), "Fracture prediction of welded steel connections using traditional fracture mechanics and calibrated micromechanics based models", *Int. J. Steel Struct.*, **11**(3), 351-366.
- Xie, Q., Li, P., Cui, Y., Sui, Y. and Su, W. (2016), "Finite element analysis of RC column-beam joint built in traditional style based on ABAQUS", *World Earthq. Eng.*, **32**(1), 245-253.
- Xue, J., Qi, L., Gao, L. and Liu, Z. (2016), "Mechanical behavior of lattice steel reinforced concrete inner frame with irregular section columns under cyclic reversed loading", *Eng. Struct.*, **128**, 225-236.
- Xue, J., Qi, L., Sui, Y. and Wu, Z. (2016), "Research on shear capacity of circle tubular steel column-double I-shaped section beam joints in imitated ancient building", *Earthq. Eng. Dyn.*, **36**(4), 192-199.
- Xue, J., Qi, L., Sui, Y., Wu, Z. and Xu, D. (2016), "Mechanical performance and shear capacity calculation of the double beam-column inner joints in steel imitated ancient building", *J. Civil. Arch. Environ. Eng.*, **38**(1), 17-22.
- Xue, J., Wu, Z., Sui, Y., Ge, H. and Wu, K. (2016), "Experimental study and numerical analysis on aseismic performance of steel

- double-beams-column interior-joints in traditional style building”, *Eng. Mech.*, **33**(5), 97-105.
- Xue, J., Zhai, L., Ma, L., Ge, H., Dong, J. and Wu, K. (2016), “Experimental study and numerical analysis on seismic behavior of steel eave columns with Dougong in imitated ancient buildings”, *China Civil Eng. J.*, **49**(7), 57-67.
- Xue, J.Y. and Qi, L.J. (2016), “Experimental studies on steel frame structures of traditional-style buildings”, *Steel Compos. Struct.*, **22**(2), 235-255.
- Yang, Y., Du, J. and Li, G. (2000), “Analysis of the earthquake disaster characteristics of ancient building structures”, *World Inform. Earthq. Eng.*, **3**.
- Yao, K., Zhao, H. and Ge, H. (2006), “Experimental studies on the characteristic of mortise-tenon joint in historic timber buildings”, *Eng. Mech.*, **23**(10), 168-172.
- Yu, M., Oda, Y., Fang, D. and Zhao, J. (2008), “Advances in structural mechanics of Chinese ancient architectures”, *Front. Arch. Civil Eng. China*, **2**(1), 1-25.
- Zhang, X. (2015), *Research on the traditional style of modern commercial buildings in Xi'an Ming City area*, Xi'an University of Architecture and Technology, Xi'an.